FRONTIERS OF PHYSICS

RESEARCH ARTICLE
Volume 21 / Issue 11 / 113202 / 2026

Vortex states trapped in alternating trapping-expulsive potentials

Zhihuan Luo[1,*], Yan Liu[1,*], Yizhang Luo[2,†], Yongyao Li[3], Josep Batle[4], Boris A. Malomed[5,6]

1 Department of Applied Physics, South China Agricultural University, Guangzhou 510642, China
2 School of Physics and Electronic Information, Guangxi Minzu University, Nanning 530006, China
3 School of Physics and Optoelectronic Engineering, Foshan University, Foshan 528000, China
4 CRISP Centre de Recerca Independent de sa Pobla, C. Albéniz 12, 07420 sa Pobla, Balearic Islands, Spain
5 Department of Physical Electronics, School of Electrical Engineering, Faculty of Engineering, and Center for Light-Matter Interaction, Tel Aviv University, Tel Aviv 69978, Israel
6 Instituto de Alta Investigación, Universidad de Tarapacá, Casilla 7D, Arica, Chile
*The two authors contributed equally to this work.
Corresponding author. E-mail: †lozit@scau.edu.cn
Received January 28, 2026; accepted March 18, 2026

© Higher Education Press 2026

ABSTRACT

We report a comprehensive analysis of dynamics of two-dimensional vortex solitons with winding number $S = 1$, maintained by a quadratic time-dependent potential with coefficient $\kappa(t) = \kappa_{\rm dc} + \kappa_{\rm ac} \cos(\omega t)$, which may periodically alternate between confinement and expulsion, in a combination with the self-focusing or defocusing cubic nonlinearity. Analytical results are reported for the linear version of the system, which is a nontrivial one too, while the nonlinear system is explored by means of systematic simulations. Fully stable axisymmetric vortex states in the system with the self-focusing nonlinearity are observed with scaled norm N taking values below a critical one, $N_{\rm cr}$. In the interval of $N_{\rm cr} < N < N_{\rm qs}$, we identify quasi-stable modes, which exhibit periodic splitting into a rotating pair of fragments and their recombination, thus breaking and restoring the axial symmetry. In the adjacent interval, $N_{\rm qs} < N < N_{\rm max}$, the system supports rotating robust states composed of two permanently separated fragments. There are no stable modes at $N > N_{\rm max}$, where the vortices are destroyed by the collapse. In the case of the self-defocusing nonlinearity, the vortices remain stable for arbitrarily large values of the norm. These findings significantly enhance the understanding of the vortex dynamics in systems subject to the time-periodic "management", which may be realized in atomic Bose–Einstein condensates and bulk optical waveguides.

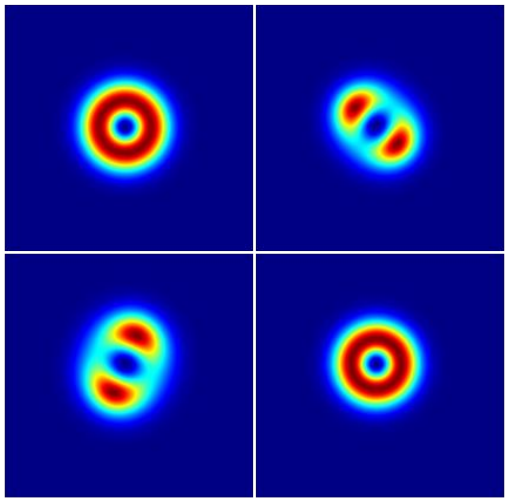

Keywords vortex state, soliton, Bose–Einstein condensates

1 Introduction

Vortex states carrying quantized angular momentum are a ubiquitous subject of current studies in the field of quantum matter – in particular, Bose–Einstein condensates (BECs) in ultracold atomic gases. While the use of permanent quadratic (harmonic-oscillator) trapping potentials facilitate the study of the nucleation, precession, and decay of two-dimensional (2D) vortices [1–6], their dynamics under the action of quadratic potentials periodically switching between confinement and expulsion remains largely unexplored. Settings with such time-

periodic "management" of the quadratic potential are now available in the experiment. For this purpose, one may use as optically painted potentials flipping the sign of the curvature on a sub-millisecond scale [7–9], as well as a pair of blue- and red-detuned laser beams [10, 11], subject to the time-periodic modulation of their intensities, with the mutual phase shift of $\pi/2$. As shown below, the application of the management drives periodically alternating cycles of compression and expansion of the BEC cloud.

In this connection, it is relevant to mention another setup, with a binary BEC composed of two Rabi-(linearly) coupled components, with one confined by the static quadratic trap, and the other subject to the action of the static expulsive (inverted) potential. The linear coupling helps to maintain stable localized 1D and 2D states in the system, against the action of the expulsive potential. It is worthy to note that stable localized vortex modes with integer winding numbers $S \geq 1$ exist in this case [12].

The advantage of the application of diverse management techniques is that they help to stabilize various species of solitons. In particular, the dispersion management fortifies solitons in optical fibers against the detrimental jitter effect [13–16]. Further, the nonlinearity management, i.e., periodic switch of the nonlinearity sign between focusing and defocusing through the Feshbach resonance by means of the ac magnetic field, is capable to effectively stabilize 2D fundamental (zero-vorticity, $S = 0$) solitons in free space against the instability driven by the occurrence of the critical collapse in this setup [17–19]. However, this mechanism cannot stabilize 2D vortex solitons against spontaneous splitting [18].

The problem of stabilizing 2D vortex and *semi-vortex* [20] solitons in BEC with the self-focusing nonlinearity was addressed by means of other methods, such as the permanent isotropic trapping potential [21–23], lattice potentials [24–26], spin-orbit coupling [20, 27], and some others [28–36], see Ref. [5] for review. In addition, lattice potentials make it possible to construct 2D stable gap solitons with embedded vorticity $S \geq 1$ in the BEC with the self-defocusing nonlinearity [37–41].

In this work, we aim to study the stability and dynamics of confined BEC vortex modes under the action of the isotropic quadratic potential, whose strength κ is subject to the periodic management, defined as

$$\kappa(t) = \kappa_{\rm dc} + \kappa_{\rm ac} \cos(\omega t), \tag{1}$$

which includes dc (constant) and ac (variable) components. The *trapping-expulsion management* (TEM) is defined by Eq. (1) with $\kappa_{\rm dc} < \kappa_{\rm ac}$, when the sign of the potential periodically alternates between the confinement and expulsion. For the zero-vorticity confined mode, the model was introduced and investigated in Ref. [42]. Here we address the states with the fundamental vorticity, $S = 1$, and produce stability charts in the plane of the TEM parameters $(\kappa_{\rm ac}, \omega)$. The interplay of TEM with the self-focusing cubic nonlinearity reveals three sharply delineated phases, depending on the mode's norm N. At $N < N_{\rm cr} \approx 7.8$ [if the nonlinearity coefficient is normalized to be $g = 1$, see Eq. (2) below], the vortex behaves as a fully stable breather: while its core radius oscillates, the vortex mode keeps its isotropic shape. Further, at $N_{\rm cr} < N < N_{\rm qs} \approx 8.5$, a quasi-stable ("qs") regime is found, in which the vortex periodically splits and recombines, the splitting-recombination period being a function of N and $\kappa_{\rm dc}$. The recombination fails at $N > N_{\rm qs}$, when the split fragments lock into a permanently rotating two-fragment state, that survives up to $N_{\rm max} \approx 9.5$. This state may be also considered as a rotating *azimuthon* [43], although azimuthons are not usually considered in systems subject to periodic time modulation. No stable states with higher vorticity, $S \geq 2$, are found; in this case, vortices quickly fission into rotating pairs of unit-charge ones, cf. Refs. [27, 39]. On the other hand, in the case of the self-defocusing nonlinearity [$g = -1$ in Eq. (2)], vortices with $S = 1$ remain stable up to indefinitely large values of the norm.

The subsequent presentation is organized as follows. The model is introduced in Section 2, where some analytical results are reported too. Results of the systematic numerical investigation are summarized in Section 3. The paper is concluded by Section 4.

2 The model and analytical considerations

Following Ref. [42], we adopt the single-component GPE, written in the scaled 2D form for the mean-field BEC wave function, ψ:

$$\mathrm{i}\frac{\partial \psi}{\partial t} = -\frac{1}{2}\nabla^2\psi - g|\psi|^2\psi + \frac{1}{2}\kappa(t) r^2 \psi, \tag{2}$$

where constant $g = +1$ or $g = -1$, with $|g| = 1$ fixed by obvious scaling of ψ (unless we set $g = 0$ in the linear model), represents, severally, the self-focusing of defocusing, r is the radial coordinate, and coefficient $\kappa(t)$ is adopted as per Eq. (1). The norm of the confined state is defined as

$$N = \int_0^\infty r\mathrm{d}r \int_0^{2\pi} \mathrm{d}\theta \left|\psi(r,\theta)\right|^2, \tag{3}$$

where θ is the angular coordinate.

The 2D model based on Eqs. (2) and (1), with t replaced by the propagation distance z, may be also realized as the nonlinear Schrödinger equation governing the light propagation in the bulk medium built as a concatenation of waveguiding and antiwaveguiding elements, which correspond to the segments with $g = +1$ and $g = -1$, respectively [44]. Formation and stability of optical solitons in the 1D waveguiding-antiwaveguiding

chain was analyzed in Ref. [45], but such models were not previously considered in 2D.

One can take the stationary version of Eq. (1) for

$$\psi = \exp(-\mathrm{i}\omega t \pm \mathrm{i}\theta)\phi(r), \tag{4}$$

with vorticity $S = \pm 1$:

$$\omega\phi = -\frac{1}{2}\left(\frac{\mathrm{d}^2}{\mathrm{d}r^2} + \frac{1}{r}\frac{d}{dr} - \frac{1}{r^2}\right)\phi - g\phi^3 + \frac{1}{2}\kappa_{\mathrm{dc}} r^2 \phi. \tag{5}$$

The angular momentum of this state is

$$M = \mathrm{i}\int_0^\infty r\mathrm{d}r \int_0^{2\pi} \mathrm{d}\theta \psi \frac{\partial}{\partial\theta}\psi^* \equiv \pm N. \tag{6}$$

Below, we focus on the vortices with $S = +1$.

Equation (5) is invariant with respect to the scaling transform,

$$(\omega, \phi, r, \kappa_{\mathrm{dc}}) \to \left(\omega' \equiv \frac{\omega}{\omega_0}, r' \equiv \sqrt{\omega_0} r, \phi' \equiv \frac{1}{\sqrt{\omega_0}}\phi, \kappa'_{\mathrm{dc}} \equiv \frac{1}{\omega_0^2}\kappa_{\mathrm{dc}}\right), \tag{7}$$

with an arbitrary positive scaling factor ω_0 (note that the transform does not change the norm, $N' \equiv N$). A straightforward consequence of Eq. (7) is

$$\frac{\omega'}{\omega} = \sqrt{\frac{\kappa'_{\mathrm{dc}}}{\kappa_{\mathrm{dc}}}}. \tag{8}$$

The square-root dependence produced by Eq. (8) provides an exact explanation for the relevant numerical results presented below.

A deeper analytical consideration is possible in the case of the nonstationary linear system, with $g = 0$ and $\kappa_{\mathrm{ac}} \neq 0$ in Eqs. (2) and (1). In this case, an exact solution for the nonstationary wave function, driven by the time-dependent potential coefficient $\kappa(t)$, is looked for as

$$\psi_{\mathrm{lin}}(r, \theta, t) = A(t) r^S \exp\left(-\mathrm{i}\chi(t) + \mathrm{i}S\theta - \frac{1}{2}a(t)r^2\right), \tag{9}$$

cf. Eq. (4), with real amplitude $A(t)$, phase $\chi(t)$, and integer vorticity $S \geq 0$ (not necessarily $S = 1$). The real and imaginary parts of the complex Gaussian parameter in this ansatz,

$$a(t) \equiv \mathrm{Re}\,(a(t)) + \mathrm{i}\,\mathrm{Im}\,(a(t)), \tag{10}$$

account for the localization of the wave function and its radial chirp [46, 47], respectively. The conserved norm of expression (9) is

$$N_{\mathrm{lin}} = \pi S! A^2 [\mathrm{Re}(a)]^{-(S+1)}. \tag{11}$$

The substitution of ansatz (9) in Eq. (2) with $g = 0$ leads to an evolution equation for $a(t)$,

$$\frac{\mathrm{d}a}{\mathrm{d}t} = \mathrm{i}\left[\kappa(t) - a^2\right], \tag{12}$$

while the evolution if $A(t)$ is determined by $\mathrm{Re}(a(t))$ through Eq. (11), and phase $\chi(t)$ evolves according to the equation

$$\frac{\mathrm{d}\chi}{\mathrm{d}t} = (S+1)\,\mathrm{Re}(a(t)). \tag{13}$$

The most important equation in this set is (12), which may be solved exactly in the case of constant κ [i.e., if $\kappa_{\mathrm{ac}} = 0$ in Eq. (1)]. This solution also provides an approximation for slowly (adiabatically) varying $\kappa(t)$ (this means that the TEM frequency is much smaller than the eigenfrequency of shape oscillations of the trapped vortex, which is discussed in detail as below):

$$a(t) \approx \sqrt{\kappa(t)}\frac{\left(\sqrt{\kappa(t)} + a_0\right)\exp\left(2\mathrm{i}\int_0^t \sqrt{\kappa(t')}\mathrm{d}t'\right) - \left(\sqrt{\kappa(t)} - a_0\right)}{\left(\sqrt{\kappa(t)} + a_0\right)\exp\left(2\mathrm{i}\int_0^t \sqrt{\kappa(t')}\mathrm{d}t'\right) + \left(\sqrt{\kappa(t)} - a_0\right)}, \tag{14}$$

where a_0 is the initial value of $a(t)$, which may be taken as a real one. In the case of $\kappa = \mathrm{const}$, the exact solution is obtained by setting $\int_0^t \sqrt{\kappa(t')}\mathrm{d}t' \to \sqrt{\kappa}t$ in Eq. (14). If the periodically varying $\kappa(t)$ becomes negative (i.e., the quadratic potential becomes expulsive), one should substitute $\sqrt{\kappa} = \mathrm{i}\sqrt{|\kappa|}$ during the corresponding part of the TEM cycle. At $t \to \infty$, the Gaussian parameter, given by Eq. (14), approaches the evident slowly varying asymptotic value,

$$a_{\mathrm{asympt}} = \sqrt{\kappa(t)}. \tag{15}$$

For $\kappa = \mathrm{const} > 0$, Eqs. (13) and (15) reproduce the commonly known eigenvalues of the 2D harmonic oscillator, $\mu = (S+1)\sqrt{\kappa}$.

To check the validity of the approximate analytical solution given by Eqs. (9)–(14), Fig. 1 displays its comparison with the numerical solution of the underlying GPE (2), in the case of $g = 0$. It is seen that the approximation is very accurate, even if the respective frequency, $\omega = 4$, is not small, hence the applicability of the asymptotic approximation is not obvious. In fact, the analytical solution also provides a good approximation for the numerical solutions of the nonlinear GPE with $|g| = 1$, provided that the norm is not too large.

In the case of $\kappa = \mathrm{const} \equiv \kappa_{\mathrm{dc}} < 0$, the asymptotic value (15) yield imaginary a_{asympt}, which implies that the stationary state is delocalized under the action of the expulsive potential. In this case, the formal solution given by Eqs. (9), (11), and (13) is irrelevant, as it corresponds to $N = \infty$. Instead, direct analysis of Eq. (5) readily provides an analytical solution with the following asymptotic form at $r \to \infty$:

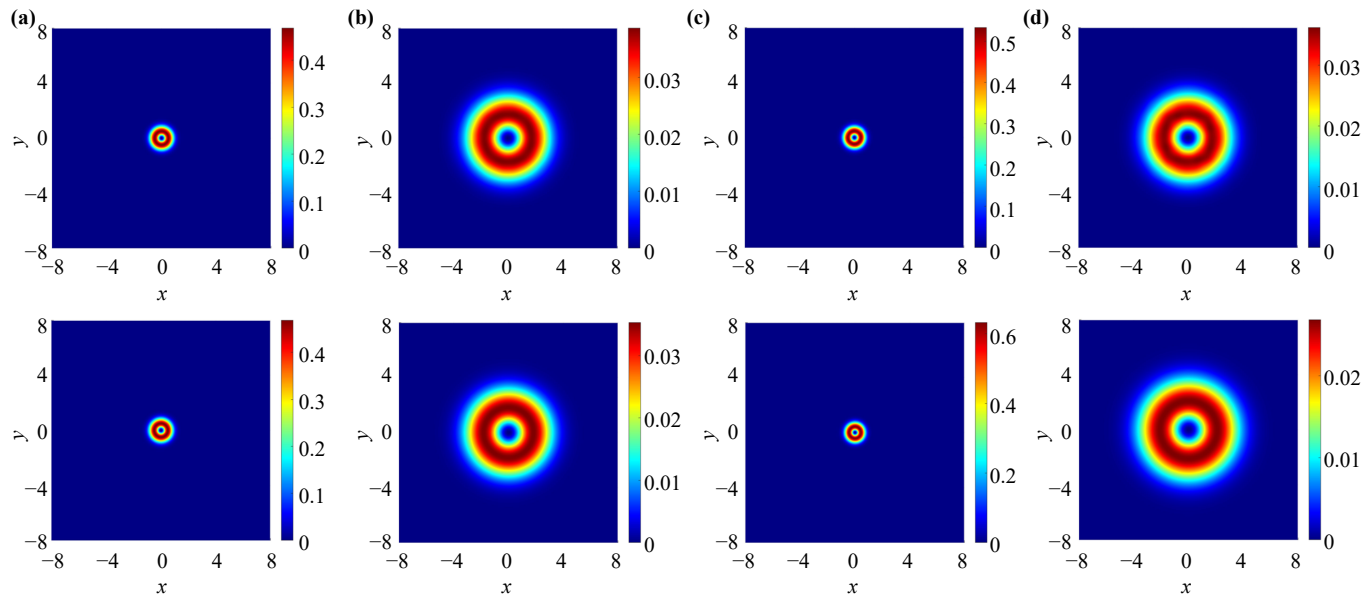

Fig. 1 The density pattern of the numerical solution of Eq. (2) (the top row) and its approximate analytical counterpart given by Eqs. (9)–(13) (the bottom row) at $t = 1$ **(a)**, $t = 200$ **(b)**, $t = 401$ **(c)**, and $t = 600$ **(d)**. The parameters are $(N, g, \kappa_{\rm dc}, \kappa_{\rm ac}, \omega) = (1, 0, 1, 0.5, 4)$ (the value of norm N is not essential for this linear solution).

$$\phi_{\rm asympt}(r) = \phi_0 r^{-1} \cos\left(\frac{r^2}{2\sqrt{|\kappa_{\rm dc}|}} + \chi_0\right), \tag{16}$$

which does not depend on chemical potential μ, nor on the vorticity, while ϕ_0 and χ_0 are real constants. In fact, expression (16) is weakly delocalized (on the contrary to an intuitive expectation that the inverted quadratic potential expel the wave function "very far" from the center), as the integral norm (3) of the asymptotic wave function (16) slowly diverges with the increase of radius R of the 2D cylindrical domain: $N \approx \pi\phi_0^2 \ln R$. In other words, the expulsive quadratic potential leads to the establishment of the stationary state (16) with amplitude $\phi_0 \approx \sqrt{N/(\pi \ln R)}$, which, in the first approximation, does not depend on strength $|\kappa_{\rm dc}|$ of the expulsive potential. In this case, the eigenvalue spectrum is continuous, admitting all real values $\mu \geq 0$ and $\mu \leq 0$.

In the general case, when the above adiabatic approximation may not apply, it is useful to split the complex equation (12), that cannot be solved exactly, into a system of real ones, by means of the substitution (10), which yields

$$\mathrm{Im}(a) = \frac{1}{2}\left[\mathrm{Re}(a)\right]^{-1} \frac{\mathrm{d}}{\mathrm{d}t}\mathrm{Re}(a), \tag{17}$$

$$\frac{\mathrm{d}^2}{\mathrm{d}t^2}\mathrm{Re}(a) = \frac{3}{2}\left[\mathrm{Re}(a)\right]^{-1}\left[\frac{\mathrm{d}}{\mathrm{d}t}\mathrm{Re}(a)\right]^2 - 2\left[\mathrm{Re}(a)\right]^3 + 2\kappa(t)\mathrm{Re}(a). \tag{18}$$

Although Eq. (18) does not admit an analytical solution, it provides details of the narrowest and widest configurations of the Gaussian core of ansatz (9): both configurations, with $\frac{\mathrm{d}}{\mathrm{d}t}\mathrm{Re}(a) = 0$, have no radial chirp, according to Eq. (17). Further, the narrowest one, corresponding to a maximum of $\mathrm{Re}(a(t))$, must have $\frac{\mathrm{d}^2}{\mathrm{d}t^2}\mathrm{Re}(a) < 0$, hence Eq. (18) demonstrates that the narrowest configuration is attained at $[\mathrm{Re}(a)]^2 > \kappa(t)$. On the other hand, the widest configuration, which corresponds to a minimum of $\mathrm{Re}(a)$, must have $\frac{\mathrm{d}^2}{\mathrm{d}t^2}\mathrm{Re}(a) > 0$, hence Eq. (17) implies $\kappa(t) > [\mathrm{Re}(a)]^2$ in this case. Thus. the widest configuration may only be attained at $\kappa(t) > 0$, when the quadratic potential in Eq. (2) is confining. This conclusion is confirmed by numerical simulations, as shown in Fig. 2. It seems counterintuitive, as one might "naively" expect the largest expansion of the Gaussian core to occur at the TEM stage with the expulsive sign of the potential, $\kappa(t) < 0$. This counterintuitive fact is also confirmed by numerical simulations for fundamental states, with $S = 0$.

3 Numerical results

In this work, we have adjusted the numerical scheme elaborated in Ref. [42]. To this end, vortical stationary solutions of Eq. (2) with $\kappa_{\rm ac} = 0$ were produced by means of the imaginary-time integration method [48–50]. Then, using the stationary solutions as inputs, simulations of the full GPE (2), including $\kappa_{\rm ac} \neq 0$, were performed by means of the usual split-step fast-Fourier-transform algorithm [50]. The system's parameters were varied to identify stable, quasi-stable, and unstable dynamical states in the course of the long-time simulations with initial conditions subjected to additive 5% random noise.

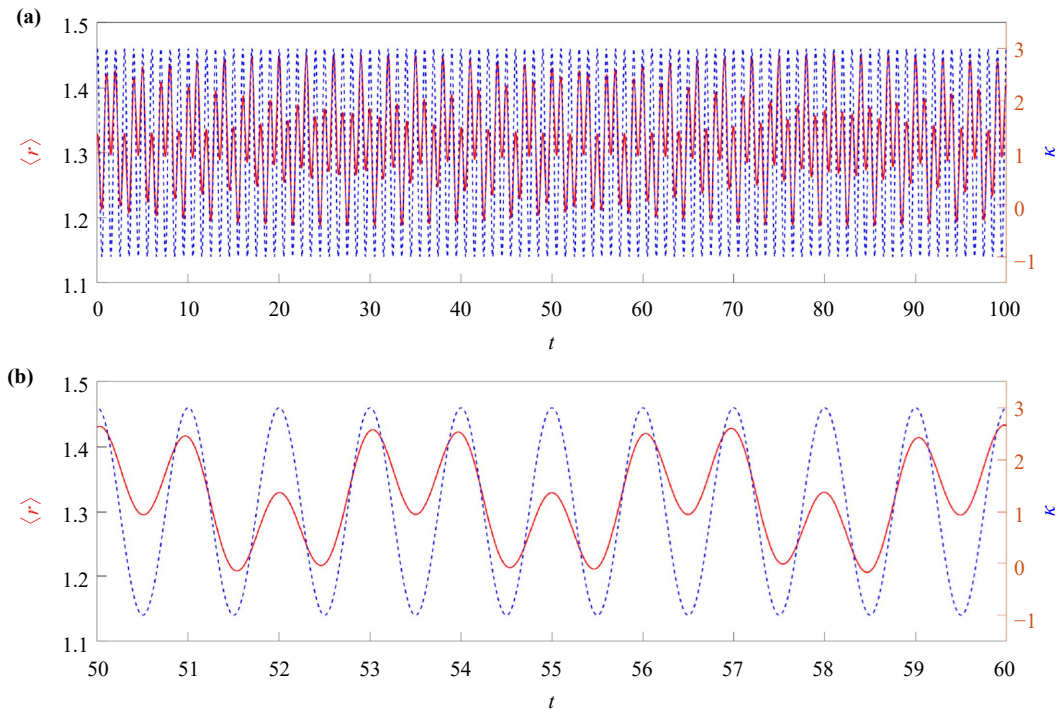

Fig. 2 **(a)** The evolution of parameter $\kappa(t)$ (the right-hand vertical axis) and radius of a stable vortex state (the left-hand vertical axis), produced by the numerical solution of the linear version of Eq. (2) with sign-varying $\kappa(t)$. **(b)** A zoomed-in view of the evolution in a shorter time interval. It is observed that, as predicted analytically, the largest values of the radius correspond to $\kappa(t) > 0$. The parameters are $(N, g, \kappa_{\rm dc}, \kappa_{\rm ac}, \omega) = (1, 0, 1, 2, 2\pi)$.

Systematic numerical simulations of Eq. (2) with the self-attractive nonlinearity, $g = +1$, reveal that the norm plays a crucial role in the stability of the vortex states with $S = 1$ under the action of TEM, while all the states with $S \geq 2$ are unstable. For values of the parameters considered in this work (see below), we have confirmed the existence of stable and quasi-stable vortex solitons with $g = +1$ and vorticity $S = 1$ within the interval

$$0 < N < N_{\rm max} \approx 9.5. \tag{19}$$

In this interval, the robustness of the vortex solitons varies, depending on the other parameters, as reported below. No stable or quasi-stable vortex states were found for $N > N_{\rm max}$ in either static traps and time-periodic potentials.

3.1 Fully stable vortex states with $S = 1$

Naturally, vortex states may be stable when norm N is not too large [23]. We have found that fully stable vortices in the case of the self-focusing nonlinearity, $g = +1$, exist in an interval

$$N < N_{\rm cr} \approx 7.8, \tag{20}$$

which is narrower than the full one (19) (the remaining part is populated by quasi-stable vortex states, see below).

The stability of the states produced by Eq. (2) for fixed N is determined by the TEM parameters $\kappa_{\rm ac}$ and ω, which are defined in Eq. (1). Figure 3 demonstrates typical examples of the stable and unstable evolution of the vortex states. In particular, for $(\kappa_{\rm ac}, \omega) = (0.5, 4)$, the radius of the vortex state periodically varies, giving rise to a dynamically stable oscillator (breather) in panel (a), with the phase distribution displayed in panel (b). On the other hand, for $(\kappa_{\rm ac}, \omega) = (0.5, 2)$, the vortex is destroyed by instability, as shown in panel (c).

Generic stability charts for the vortex solitons in the $(\kappa_{\rm ac}, \omega)$ plane, in the case of the self-focusing nonlinearity $(g = +1)$, are presented in Figs. 4(a) and (b). The vortices are stable beneath the lower boundaries and above the upper ones. In cases of the sign-changing potential strength, i.e., $\kappa_{\rm ac} > \kappa_{\rm dc}$ in Eq. (1), the lower stability area disappears, whereas the upper ones persists. This is possible because rapid alternations corresponding to large TEM frequencies ω, in the upper area, may help to mitigate the destructive effect of the evolution stages in which the potential is expulsive, while this stabilization mechanism does not act in the lower area. Sharp jumps of the lower boundaries in panels (a) and (b) correspond to discrete transitions in the number of modulation periods required for vortex splitting, reflecting the quasi-periodic nature of the splitting-recombination dynamics. Below, we present the findings for $\kappa_{\rm ac} < \kappa_{\rm dc}$, as the results obtained in the

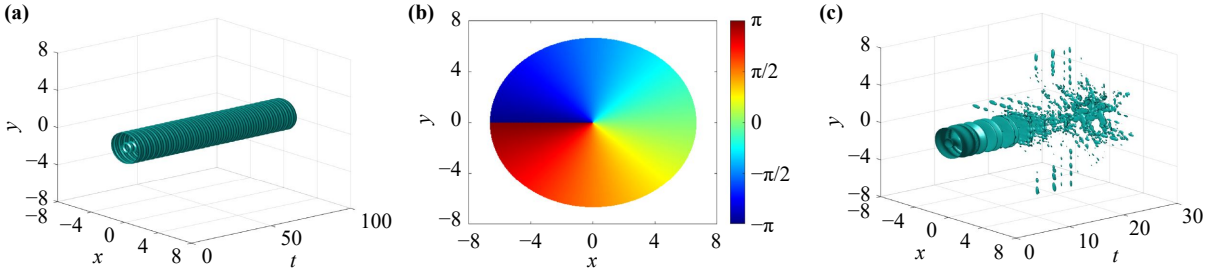

Fig. 3 **(a)** and **(b)** show the evolution and phase distribution, respectively, of a typical stable vortex state for parameters $(\kappa_{ac}, \omega) = (0.5, 4)$. **(c)** illustrates the evolution of a typical unstable state for $(\kappa_{ac}, \omega) = (0.5, 2)$. The other parameters are $(N, \kappa_{dc}) = (1, 1)$, and $g = +1$ (the self-focusing nonlinearity).

upper stability area feature no essential difference between the cases $\kappa_{ac} < \kappa_{dc}$ and $\kappa_{ac} > \kappa_{dc}$.

In the limit of $\kappa_{ac} \to 0$, the upper and lower stability boundaries meet at the resonance point, denoted by ω_{res} in Figs. 4(a, b). This is explained by the fact that the ac term, with a small amplitude κ_{ac}, resonates with an intrinsic mode of the vortex state in the stationary setup, which was found in earlier studies [23]. The resonant frequency ω_{res} represents the eigenfrequency of small oscillations of the radial width around its equilibrium value, for the vortex trapped in the stationary potential. When the modulation frequency approaches this value, the external forcing can resonantly enhance the breathing dynamics. It is relevant to mention that the interplay of the cubic nonlinearity with the stationary trapping potential may produce higher-order eigenfrequencies of small oscillations. The possibility of the resonance at the higher eigenfrequencies, produced by the application of the management, may be a subject for an additional work. This resonant point shifts upward with the increase of κ_{dc}, as seen in Fig. 4(c). As explained above and shown in Fig. 4(c), this feature is exactly explained by the analytical result Eq. (8), which is based on the scaling argument.

The stability charts for different values of norm N in the system with the self-focusing nonlinearity, $g = +1$, are collected in Fig. 5. The upper stability boundaries for different norms are nearly identical, whereas the lower ones exhibit small deviations at relatively large values of κ_{ac}. Thus, within the range shown in Eq. (20), the weak dependence on the norm implies that the stability of the vortices with $S = 1$ is dominated by the linear part of the underlying equation (1), akin to the situation for the trapped states with $S = 0$ reported in Ref. [42].

The fact that the stability in the present range is chiefly determined by the linear properties of the model is clearly corroborated by the stability charts plotted in Fig. 5(b) for a fixed norm $(N = 1)$ and values of the nonlinearity coefficient $g = +1$, -1, and 0 in Eq. (1). It is observed that stability areas for either sign of the nonlinearity, $g = \pm 1$, is indeed nearly identical to the one in the linear system, with $g = 0$.

The situation is drastically different at $N > N_{cr}$, in which case the vortices develop dynamical instability in the self-focusing system, $g = +1$, as shown in detail below. On the contrary, with $g = -1$ (self-defocusing) the vortices remain stable for arbitrarily large values of N.

3.2 Quasi-stable vortex states with $S = 1$ and $g = +1$ (self-focusing nonlinearity)

Further numerical analysis reveals that, in a relatively

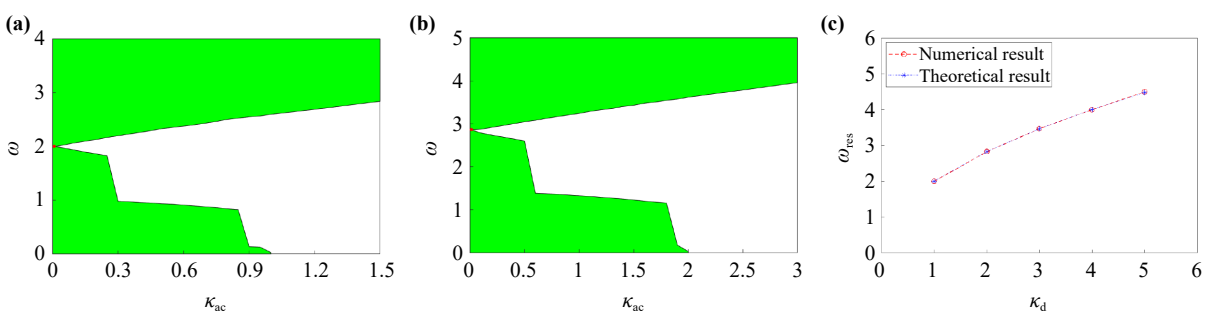

Fig. 4 **(a)** The stability chart for the vortex state in the (κ_{ac}, ω) plane for $\kappa_{dc} = 1$. The vortex is stable in the green areas and unstable in the white one between them. The upper and lower stability boundaries meet at the resonance point, $\omega_{res} = 2.00$. **(b)** The the same as in (a), but for $\kappa_{dc} = 2$, resulting in $\omega_{res} = 2.83$, in agreement with Eq. (8). **(c)** The resonance values ω_{res} vs. κ_{dc}, as produced by the numerical findings and analytical result (8), which are in complete agreement. The other parameters are $N = 1$ and $g = +1$ (the self-focusing sign of the nonlinearity).

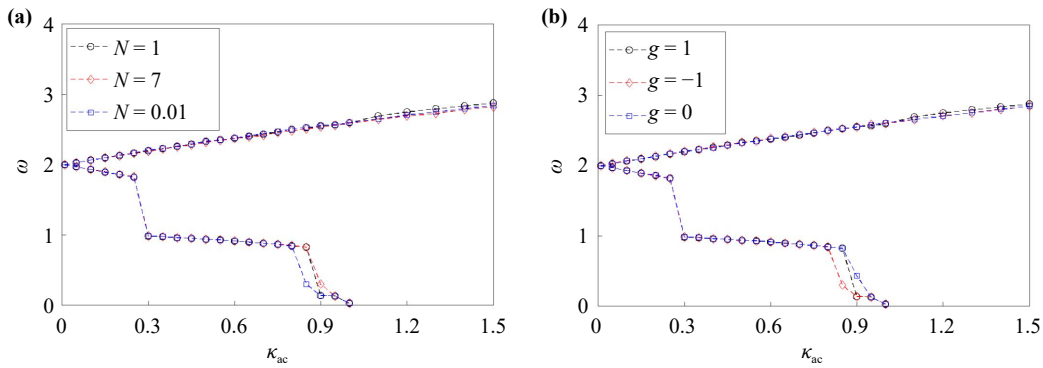

Fig. 5 Stability charts in the $(\kappa_{\rm ac}, \omega)$ plane for different norms N, self-focusing sign of the nonlinearity $(g = +1)$, and fixed $\kappa_{\rm dc} = 1$ **(a)**, and for different values of the nonlinearity coefficient, $g = \pm 1$ and 0, keeping fixed values $(N, \kappa_{\rm dc}) = (1, 1)$ **(b)**.

narrow interval of the norm values,

$$N_{\rm cr} < N < N_{\rm qs} \approx 8.5, \tag{21}$$

the vortices with $S = 1$ exist but exhibit a behavior distinct from that of the stable axisymmetric oscillating states. The vortices periodically break the axial symmetry, spontaneously splitting into a rotating pair of fragments, which then recombine to restore the original vortex. We define such periodically splitting and recombining vortex states as *quasi-stable* ones, to distinguish them from the stable axial-symmetry-preserving states, which are reported above. To verify the robustness of these states, we perturbed the initial condition with additive random noise at the 5% amplitude level, and performed long-time simulations, up to $t \sim 10^4$ in the scaled units, confirming that the quasi-stable vortex structure persists throughout the evolution. The periodic cycle of the fission and fusion of the quasi-stable vortices is illustrated by the set of snapshots displayed in Fig. 6. The rotation of the pair of the fragments is seen in panels (b) and (c), while the intensity distributed in different quadrants is always symmetric with respect to the origin (rotation pivot). The magnitude and sign of the rotation angular velocity are determined by the conservation of the angular momentum [see Eq. (6)], hence the quasi-stable vortex state with $S = -1$ (instead of $S = +1$ considered above) periodically splits into the pair of fragments rotating in the opposite direction.

As the intensity distribution of the quasi-stable mode keeps its symmetry with respect to the origin, the intensity weights of different quadrants can be utilized to identify the particular state as a full vortex or a two-fragment form. Figure 7 displays a typical instance of the evolution of the intensity weights in the first and second quadrants for the quasi-stable state, with periodically oscillating intensity weights. Note that the respective rotation frequency, which is determined by the fixed value (6) of the input angular momentum, is ≈ 7 times larger than the frequency of fission-fusion cycle.

The splitting-recombination period of the quasi-stable state depends on norm N and TEM parameter $\kappa_{\rm dc}$, as shown in Fig. 8. With the increase of N and $\kappa_{\rm dc}$, the splitting-recombination period decreases, as the effective nonlinearity and confinement, which drive this process, become stronger. The rotation period of the two-fragment form is plotted vs. N and $\kappa_{\rm dc}$ in panels (c) and (d), respectively, indicating that the rotation period weakly depends on N but decreases with the increase of $\kappa_{\rm dc}$.

The persistence boundaries for the quasi-stable states have been carefully analyzed, as reported in Fig. 9. These findings bear a close resemblance to the stability boundaries for the fully stable vortices, which are presented above in Fig. 5, suggesting a consistent

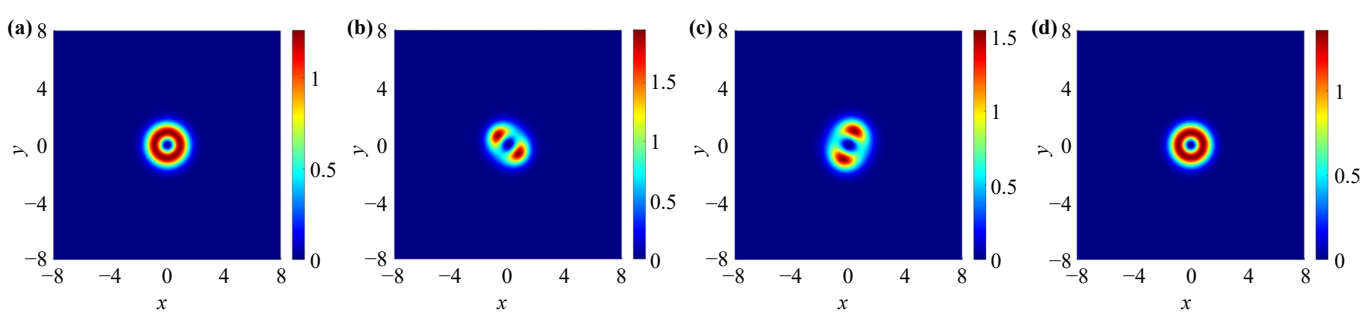

Fig. 6 Snapshots of the density profile of a quasi-stable vortex, illustrating its periodic fission and fusion in the self-focusing system $(g = +1)$: **(a)** $t = 5.0$, **(b)** $t = 26.5$, **(c)** $t = 33.2$, **(d)** $t = 60.0$. The parameters are $(N, \kappa_{\rm dc}, \kappa_{\rm ac}, \omega) = (8, 1, 0.5, 4)$.

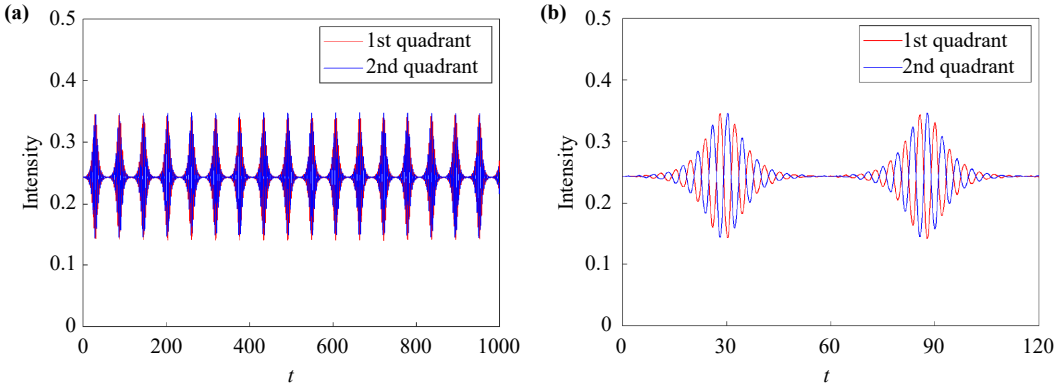

Fig. 7 **(a)** The evolution of the intensity weights of the quasi-stable state in the first and second quadrants. **(b)** A zoomed-in view of the evolution in a shorter time interval. The angular velocity of the rotating two-fragment form is 0.74 rad/s, whereas the angular frequency of the fission-fusion cycles is much lower, 0.11 rad/s. The parameters are $(N, g, \kappa_{\rm dc}, \kappa_{\rm ac}, \omega) = (8, +1, 1, 0.5, 4)$.

pattern in the behavior of the stable and quasi-stable states in broad parameter areas.

3.3 Other vortex states with $S = 1$ and $g = +1$

With the growth of the norm, the distance between the separated fragments of the quasi-stable states increases. When the norm attains the value $N_{\rm qs} \approx 8.5$, the adjacent fragments cease to overlap, resulting in a rotating state that keeps the two-fragment form without recombination. Figure 10 shows a typical example of the permanently separated pair of fragments, which persists and keeps rotating, so as to conserve the initial angular momentum (6). In panel (a), the intensity weights of the first and second quadrants are not equal, indicating that the two fragments do not recombine. Snapshots of this permanently separated state are displayed in panels (b)–(d). It persist up to $N = N_{\rm max} \approx 9.5$, above which the state becomes fully unstable. Figure 11 reports the stability chart for values of N below and close to $N_{\rm max}$. As N approaches $N_{\rm max}$, the stability area shrinks and eventually vanishes at $N = N_{\rm max}$. A typical example of the unstable evolution for $N = 9.6$, slightly above $N_{\rm max}$, is illustrated in Fig. 12, where a typical collapse scenario is observed.

It is relevant to briefly estimate the applicability of the predicted results for experimental implementation in BEC. For the condensate of $\sim 10^4$ ^{7}Li atoms, with the radial trap frequency $\omega_r = 2\pi \times 100$ Hz and atom number, values of the scaledg norm $N \sim 5$ are experimentally feasible. The time-modulation frequency of the trapping potential, $\Omega \sim \omega_r$, lies within accessible experimental ranges.

3.4 Vortex states with $S \geq 2$

In this work, we do not address higher-order vortex states, as no stable vortices with $S \geq 2$ have been found in the case of the self-focusing nonlinearity $(g = +1)$ (while they may be stable under the action of the self-defocusing, $g = -1$). Preliminary results indicate that, in the case of $S = 2$ and $g = +1$, the system may instead maintain a rotating pair of permanently separated vortices, each carrying $S = 1$. This type of the excited vortex states is currently under investigation and will be reported elsewhere.

4 Conclusion

By systematically charting the existence and stability

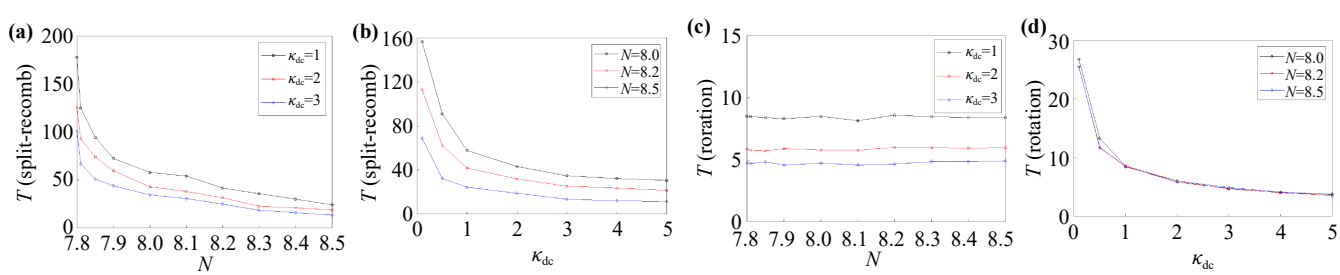

Fig. 8 **(a)** The period of the splitting-recombination of the quasi-stable states vs. norm N. **(b)** The splitting-recombination period vs. $\kappa_{\rm dc}$. **(c)** The rotation period of the two-fragment form vs. N. **(d)** The rotation period vs. $\kappa_{\rm dc}$. The parameters are $(N, g, \kappa_{\rm ac}, \omega) = (8.0, +1, 0.5, 4.0)$.

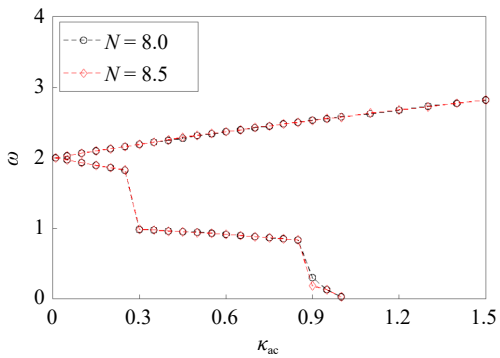

Fig. 9 The persistence boundaries for quasi-stable states in the $(\kappa_{\rm ac}, \omega)$ plane for different norms N, in the case of the self-focusing nonlinearity $(g = +1)$ and $\kappa_{\rm dc} = 1$.

areas for the vortex states with $S = 1$, under the action of the time-modulated isotropic quadratic potential, which may periodically flip between confinement and expulsion, we have closed a gap in the understanding of how topological solitons respond to the application of TEM (trapping-expulsion management). Three norm-controlled dynamical regimes have been thus identified, focusing on the case of the self-attractive nonlinearity: the truly stable breathers with norms $N < 7.8$, the periodically splitting and recombining, and also rotating, quasi-stable states at $7.8 < N < 8.5$, and rotating permanently separated states at $8.5 < N < 9.5$. Stability boundaries of these regimes are plotted in the parameter planes, underscoring the universal character of the underlying parametric resonance, which determines the point at which the stability boundaries commence. All higher-order vortices are unstable, splitting into sets of unitary vortices.

Our results suggest a previously unexplored route to the creation of topologically protected pulsating modes, that may be used, in particular, as data carriers. In this context, the quasi-stable periodically splitting and recombining states exhibit predictable windows in which the vortex-encoded phase can be read out before the next recombination. Thus, the scheme offers a natural clock for the coherent readout.

The predicted regimes can be realized experimentally in available BEC setups using ultracold gases of ^{39}K [51] or ^{7}Li [52] atoms, by ramping the scattering length of the attractive atomic interaction into the $-10a_0 \sim -100a_0$ range ($a_0 \approx 0.053$ nm is the Bohr radius), and modulating the optical quadratic potential at kHz frequencies. On the other hand, pushing the condensate beyond

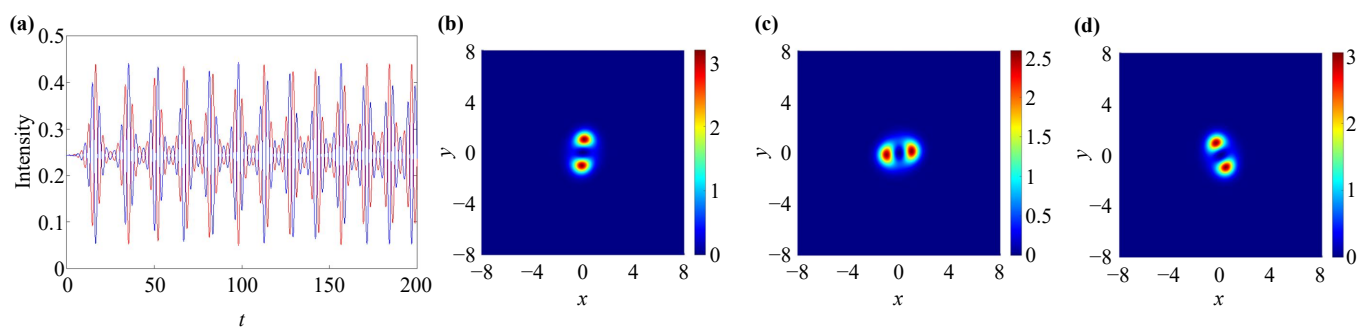

Fig. 10 **(a)** The evolution of the intensity weights of a permanently separated vortex state in the first (red) and second (blue) quadrants, in the case of $g = +1$ (the self-focusing nonlinearity). Snapshots of the permanently separated states in the course of the evolution: **(b)** $t = 300$, **(c)** $t = 600$, **(d)** $t = 900$. The angular velocity of the rotation is 0.75 rad/s. The parameters are $(N, \kappa_{\rm dc}, \kappa_{\rm ac}, \omega) = (8.8, 1, 0.5, 4.0)$.

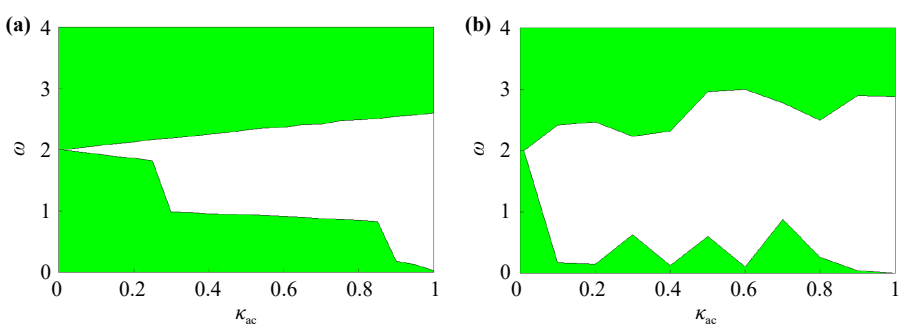

Fig. 11 The stability charts for the permanently separated rotating pair of fragments in the plane of $(\kappa_{\rm ac}, \omega)$ at values of the norm $N = 9.3$ in **(a)** and 9.4 in **(b)**. Stability areas are painted green. Other parameters are $(g, \kappa_{\rm dc}) = (+1, 1)$. No stable state was found for $N > 9.5$.

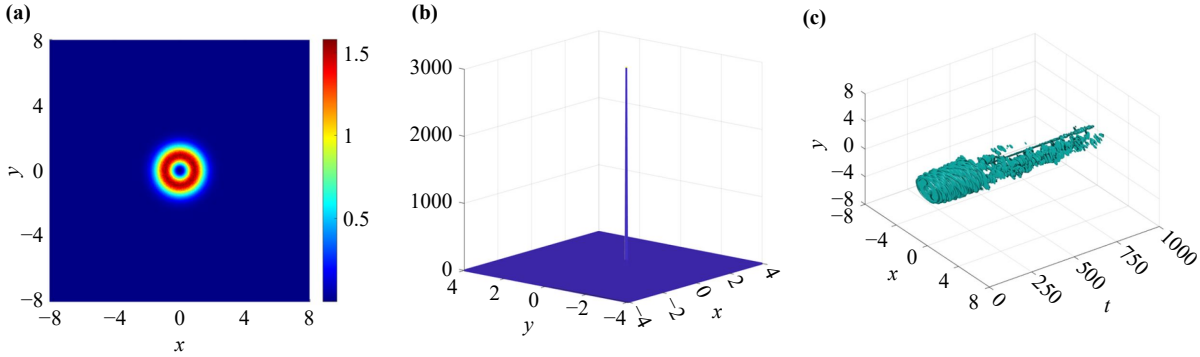

Fig. 12 An unstable vortex state with $S = 1$ and $g = +1$ (the self-focusing nonlinearity). **(a)** The input density profile of the state at $t = 0$, with a small perturbation. **(b)** The collapsed state at $t = 1000$. **(c)** The evolution of the unstable vortex state. The parameters are $(N, \kappa_{\rm dc}, \kappa_{\rm ac}, \omega) = (9.6, 1, 0.5, 4)$.

$N_{\max} \approx 9.5$ triggers the collapse in the self-attractive BEC, a regime in which the interplay of the three-body loss and TEM may create dissipative vortex lattices, cf. Ref. [53]. Extending the TEM protocol to anisotropic or annular settings may help to stabilize higher-order vortices, offering a possibility to discover new dynamical modes in quantum gases [27, 41]. A similar setting may be realized in a bulk waveguiding-antiwaveguiding system in nonlinear optics. Thus, the results reported here demonstrate that TEM enables the use the quadratic potential as a tool for the realization of controllable soliton metamorphoses.

Declarations The authors declare that they have no competing interests and there are no conflicts.

Acknowledgements This work was supported by the National Natural Science Foundation of China (Grant Nos. 12274077 and 22574057).

References

1. M. Quiroga-Teixeiro and H. Michinel, Stable azimuthal stationary state in quintic nonlinear optical media, *J. Opt. Soc. Am. B* 14(8), 2004 (1997)
2. L. Bergé, Wave collapse in physics: Principles and applications to light and plasma waves, *Phys. Rep.* 303(5–6), 259 (1998)
3. C. Sulem and P. L. Sulem, The Nonlinear Schrödinger Equation: Self-Focusing and Wave Collapse, Springer, New York, 1999
4. G. Fibich, The Nonlinear Schrödinger Equation: Singular Solutions and Optical Collapse, Springer, Heidelberg, 2015
5. B. A. Malomed, Vortex solitons: Old results and new perspectives, *Physica D* 399, 108 (2019)
6. G. D. Montesinos, V. M. Pérez-Garcia, and P. J. Torres, Stabilization of solitons of the multidimensional nonlinear Schrödinger equation: Matter-wave breathers, *Physica D* 191(3–4), 193 (2004)
7. K. Henderson, C. Ryu, C. MacCormick, and M. G. Boshier, Experimental demonstration of painting arbitrary and dynamic potentials for Bose–Einstein condensates, *New J. Phys.* 11(4), 043030 (2009)
8. M. Lacki, P. Zoller, and M. A. Baranov, Stroboscopic painting of optical potentials for atoms with subwavelength resolution, *Phys. Rev. A* 100(3), 033610 (2019)
9. G. Condon, M. Rabault, B. Barrett, L. Chichet, R. Arguel, H. Eneriz-Imaz, D. Naik, A. Bertoldi, B. Battelier, P. Bouyer, and A. Landragin, All-optical Bose–Einstein condensates in microgravity, *Phys. Rev. Lett.* 123(24), 240402 (2019)
10. F. Le Kien, V. I. Balykin, and K. Hakuta, State-insensitive trapping and guiding of cesium atoms using a two-color evanescent field around a subwavelength-diameter fiber, *J. Phys. Soc. Jpn.* 74(3), 910 (2005)
11. A. Goban, K. S. Choi, D. J. Alton, D. Ding, C. Lacroûte, M. Pototschnig, T. Thiele, N. P. Stern, and H. J. Kimble, Demonstration of a state-insensitive, compensated nanofiber trap, *Phys. Rev. Lett.* 109(3), 033603 (2012)
12. N. Hacker and B. A. Malomed, Trapping wave fields in an expulsive potential by means of linear coupling, *Phys. Rev. E* 105(3), 034213 (2022)
13. N. J. Smith, F. M. Knox, N. J. Doran, K. J. Blow, and I. Bennion, Enhanced power solitons in optical fibres withperiodic dispersion management, *Electron. Lett.* 32(1), 54 (1996)
14. A. Berntson, N. Doran, W. Forysiak, and J. Nijhof, Power dependence of dispersion-managed solitons for anomalous, zero and normal path-average dispersion, *Opt. Lett.* 23(12), 900 (1998)
15. B. A. Malomed, Soliton Management in Periodic Systems, Springer, New York, 2006
16. S. K. Turitsyn, B. G. Bale, and M. P. Fedoruk, Dispersion-managed solitons in fibre systems and lasers, *Phys. Rep.* 521(4), 135 (2012)
17. I. Towers and B. A. Malomed, Stable (2+1)-dimensional solitons in a layered medium with sign-alternating Kerr nonlinearity, *J. Opt. Soc. Am. B* 19(3), 537 (2002)
18. F. Kh. Abdullaev, J. G. Caputo, R. A. Kraenkel, and B. A. Malomed, Controlling collapse in Bose–Einstein condensation by temporal modulation of the scattering length, *Phys. Rev. A* 67(1), 013605 (2003)
19. H. Saito and M. Ueda, Dynamically stabilized bright

solitons in a two-dimensional Bose–Einstein condensate, *Phys. Rev. Lett.* 90(4), 040403 (2003)
20. H. Sakaguchi, B. Li, and B. A. Malomed, Creation of two-dimensional composite solitons in spin–orbit-coupled self-attractive Bose–Einstein condensates in free space, *Phys. Rev. E* 89(3), 032920 (2014)
21. J. R. Dodd, Approximate solutions of the nonlinear Schrödinger equation for ground and excited states of Bose–Einstein condensates, *J. Res. Natl. Inst. Stand. Technol.* 101(4), 545 (1996)
22. T. J. Alexander and L. Bergé, Ground states and vortices of matter-wave condensates and optical guided waves, *Phys. Rev. E* 65(2), 026611 (2002)
23. D. Mihalache, D. Mazilu, B. A. Malomed, and F. Lederer, Vortex stability in nearly-two-dimensional Bose–Einstein condensates with attraction, *Phys. Rev. A* 73(4), 043615 (2006)
24. B. B. Baizakov, B. A. Malomed, and M. Salerno, Multi-dimensional solitons in periodic potentials, *Europhys. Lett.* 63(5), 642 (2003)
25. J. Yang and Z. H. Musslimani, Fundamental and vortex solitons in a two-dimensional optical lattice, *Opt. Lett.* 28(21), 2094 (2003)
26. Z. Tan, H. Gong, B. Zhu, H. Zhong, and S. Hu, Two-dimensional anisotropic vortex-bright soliton and its dynamics in dipolar Bose–Einstein condensates in optical lattice, *Nonlinear Dyn.* 111(10), 9467 (2023)
27. V. E. Lobanov, Y. V. Kartashov, and V. V. Konotop, Fundamental, multipole, and half-vortex gap solitons in spin-orbit coupled Bose–Einstein condensates, *Phys. Rev. Lett.* 112(18), 180403 (2014)
28. K. Mukherjee, S. Mistakidis, P. G. Kevrekidis, and P. Schmelcher, Quench induced vortex-bright-soliton formation in binary Bose–Einstein condensates, *J. Phys. At. Mol. Opt. Phys.* 53(5), 055302 (2020)
29. W. Wang, Controlled engineering of a vortex-bright soliton dynamics using a constant driving force, *J. Phys. At. Mol. Opt. Phys.* 55(10), 105301 (2022)
30. A. Paredes, J. Blanco-Labrador, D. N. Olivieri, J. R. Salgueiro, and H. Michinel, Vortex revivals and Fermi-Pasta–Ulam–Tsingou recurrence, *Phys. Rev. E* 99(6), 062211 (2019)
31. S. L. Xu, M. R. Belić, D. P. Cai, L. Xue, J. R. He, and J. Cheng, Vortex solitons produced in spatially modulated linear and nonlinear refractive index waveguides, *J. Opt. Soc. Am. B* 35(2), 410 (2018)
32. J. R. Salgueiro, M. Zacarés, H. Michinel, and A. Ferrando, Vortex replication in Bose–Einstein condensates trapped in double-well potentials, *Phys. Rev. A* 79(3), 033625 (2009)
33. A. Paredes, J. R. Salgueiro, and H. Michinel, On vortex and dark solitons in the cubic–quintic nonlinear Schrödinger equation, *Physica D* 437, 133340 (2023)
34. L. Xue, J. He, Z. Hu, and Q. Zhang, Vortex solitons in nonlinear media with radial power-law traps and potential wells under the modulation of spatially inhomogeneous nonlinearities, *Chaos Solitons Fractals* 202(Part 2), 117576 (2026)
35. C. F. Sánchez, A. Paredes, H. Michinel, B. A. Malomed, and J. R. Salgueiro, Guided vortex bullets, *Phys. Rev. Lett.* 136(3), 033802 (2026)
36. N. K. Efremidis, K. Hizanidis, B. A. Malomed, and P. Di Trapani, Three-dimensional vortex solitons in self-defocusing media, *Phys. Rev. Lett.* 98(11), 113901 (2007)
37. E. A. Ostrovskaya and Y. S. Kivshar, Matter-wave gap vortices in optical lattices, *Phys. Rev. Lett.* 93(16), 160405 (2004)
38. H. Sakaguchi and B. A. Malomed, Two-dimensional loosely and tightly bound solitons in optical lattices and inverted traps, *J. Phys. At. Mol. Opt. Phys.* 37(11), 2225 (2004)
39. C. Huang, L. Dong, H. Deng, X. Zhang, and P. Gao, Fundamental and vortex gap solitons in quasiperiodic photonic lattices, *Opt. Lett.* 46(22), 5691 (2021)
40. X. Liu and J. Zeng, Matter-wave gap solitons and vortices of dense Bose–Einstein condensates in moiré optical lattices, *Chaos Solitons Fractals* 174, 113869 (2023)
41. C. Li, L. Dong, H. Deng, X. Zhang, and P. Gao, Gap solitons and vortices in two-dimensional spin–orbit-coupled Bose- Einstein condensates loaded onto moiré optical lattices, *Quantum Front.* 2, 1 (2025)
42. Z. Luo, Y. Liu, Y. Li, J. Batle, and B. A. Malomed, Stability limits for modes held in alternating trapping-expulsive potentials, *Phys. Rev. E* 106(1), 014201 (2022)
43. A. S. Desyatnikov, A. A. Sukhorukov, and Y. S. Kivshar, Azimuthons: Spatially modulated vortex solitons, *Phys. Rev. Lett.* 95(20), 203904 (2005)
44. B. V. Gisin and A. A. Hardy, Stationary solutions of plane nonlinear optical antiwaveguides, *Opt. Quantum Electron.* 27(6), 565 (1995)
45. A. Kaplan, B. V. Gisin, and B. A. Malomed, Stable propagation and all-optical switching in planar waveguide –antiwaveguide periodic structures, *J. Opt. Soc. Am. B* 19(3), 522 (2002)
46. I. Chremmos, N. K. Efremidis, and D. N. Christodoulides, Pre-engineered abruptly autofocusing beams, *Opt. Lett.* 36(10), 1890 (2011)
47. M. Yessenov, J. Free, Z. Z. Chen, E. G. Johnson, M. P. J. Lavery, M. A. Alonso, and A. F. Abouraddy, Space-time wave packets localized in all dimensions, *Nat. Commun.* 13(1), 4573 (2022)
48. M. L. Chiofalo, S. Succi, and M. P. Tosi, Ground state of trapped interacting Bose–Einstein condensates by an explicit imaginary time algorithm, *Phys. Rev. E* 62(5), 7438 (2000)
49. W. Bao and Q. Du, Computing the ground state solution of Bose–Einstein condensates by a normalized gradient flow, *SIAM J. Sci. Comput.* 25(5), 1674 (2004)
50. J. Yang, Nonlinear Waves in Integrable and Nonintegrable Systems, SIAM, Philadelphia, 2010
51. G. Roati, M. Zaccanti, C. D'Errico, J. Catani, M. Modugno, A. Simoni, M. Inguscio, and G. Modugno, ^{39}K Bose–Einstein condensate with tunable interactions, *Phys. Rev. Lett.* 99(1), 010403 (2007)
52. S. E. Pollack, D. Dries, M. Junker, Y. P. Chen, T. A. Corcovilos, and R. G. Hulet, Extreme tunability of interactions in a ^{7}Li Bose–Einstein condensate, *Phys. Rev. Lett.* 102(9), 090402 (2009)
53. T. W. Chen, S. D. Jheng, T. F. Jiang, and S. C. Cheng, Quantum fluctuations and stability of vortex lattices in a nonresonantly pumped exciton–polariton condensate, *J. Phys.: Condens. Matter* 29(8), 085403 (2017)